Electronic Supplementary Material (ESI) for Physical Chemistry Chemical Physics.

Electronic Supporting Information for:

"Local structure and composition of PtRh nanoparticles produced through cathodic corrosion"

Thomas J.P. Hersbach, Ruud Kortlever, Matti Lehtimäki, Petr Krtil, Marc T.M. Koper

EXAFS functions in R-space

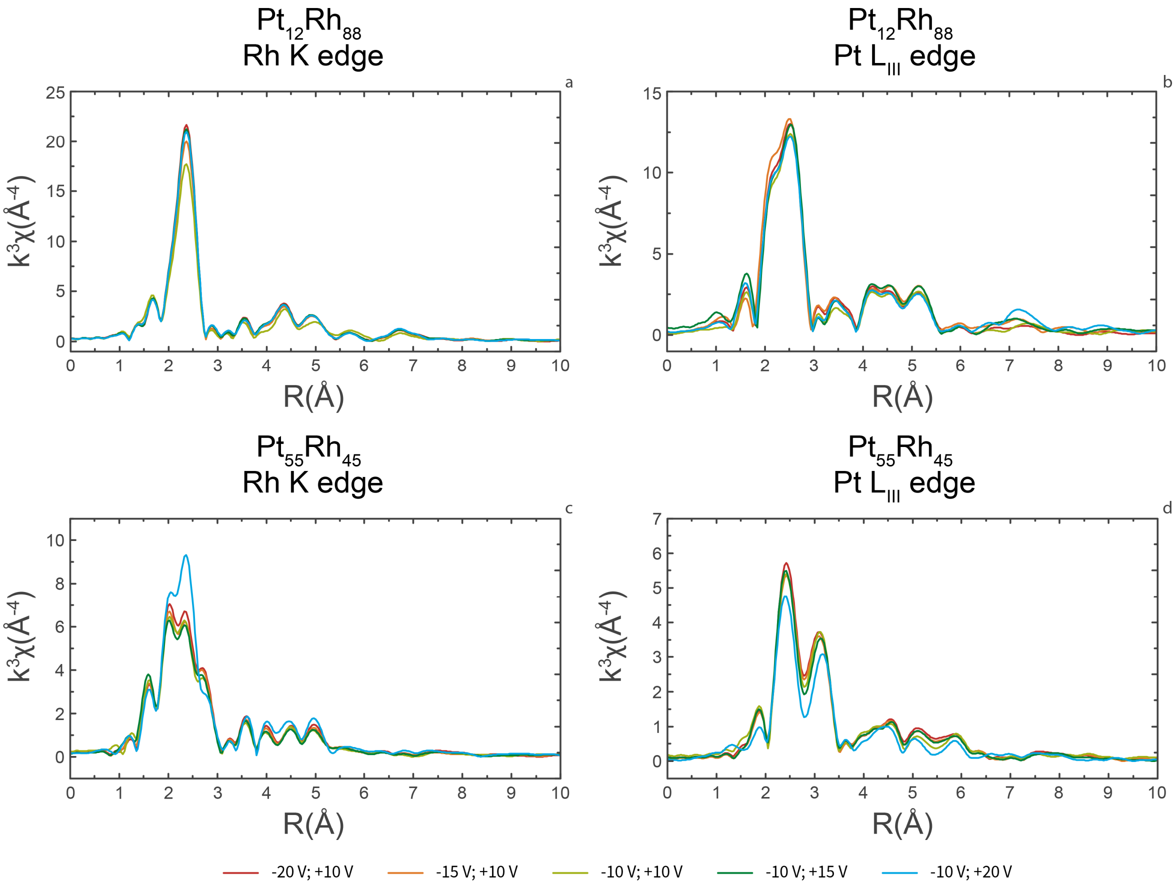

Fig. S1: EXAFS functions in R-space for the Rh K edge of $Pt_{12}Rh_{88}$ particles (a), the Pt L_{III} edge of $Pt_{12}Rh_{88}$ particles (b), the Rh K edge of $Pt_{55}Rh_{45}$ particles (c) and the Pt L_{III} edge of $Pt_{55}Rh_{45}$ particles (d), prepared at various potentials.

Nanoparticle X-ray diffraction patterns

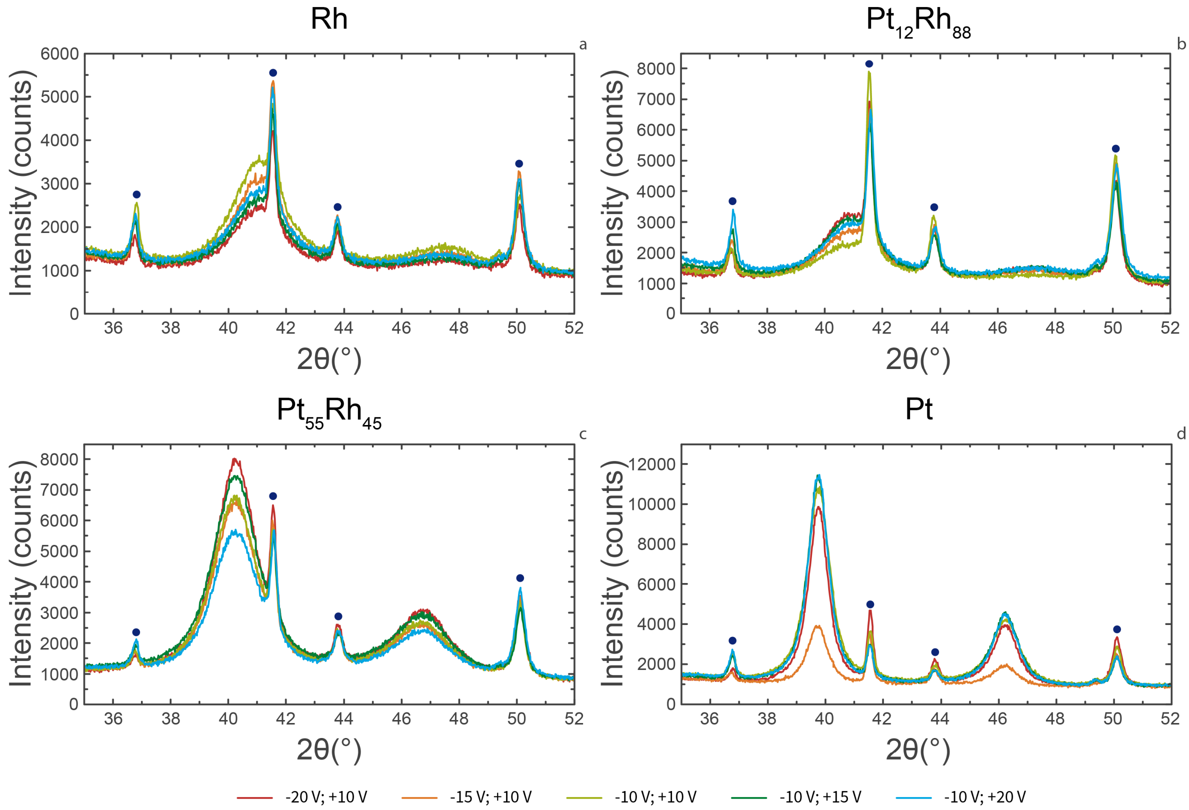

Fig. S2: X-ray diffraction patterns of Rh (a), $Pt_{12}Rh_{88}$ (b), $Pt_{55}Rh_{45}$ (c) and Pt (d) particles, prepared at various potentials. Peaks marked with a circle correspond to boron nitride reflections.

Particle sizes as determined by transmission electron microscopy

Transmission electron microscopy (TEM) samples were prepared by mixing a droplet of nanoparticle suspension with 1.5 mL of ethanol (Sigma-Aldrich, puriss. p.a.). This mixture was then applied on a TEM grid (Formvar film on copper 300 mesh) and subsequently air-dried. All TEM data were obtained using a JEOL TEM 1010. Average particle sizes and size standard deviations, given in Table S1, were calculated by analyzing 200 particles per sample. Particle size distributions for Rh, $Pt_{12}Rh_{88}$, $Pt_{55}Rh_{45}$ and Pt were generated by analyzing the same 200 particles per sample. These distributions are displayed in Fig. S3, Fig. S4, Fig. S5, and Fig. S6, respectively. If agglomerated particles were present, these particles were not treated as one large particle. Rather, the individual primary crystallites were counted as individual particles, in order to facilitate a direct comparison with the X-ray diffraction-based coherent domain sizes.

Table S1: Average particle sizes and standard deviations for all alloys and potential limits.

Potential Limits	Rh particle size (nm)	$Pt_{12}Rh_{88}$ particle size (nm)	$Pt_{55}Rh_{45}$ particle size (nm)	Pt particle size (nm)
-20 V; +10 V	2.5 ± 0.7	1.9 ± 0.4	3.9 ± 0.8	17 ± 6
-15 V; +10 V	2.2 ± 1.0	2.2 ± 0.7	2.8 ± 1.0	3.4 ± 2.1
-10 V; +10 V	1.3 ± 0.5	1.8 ± 0.7	3.0 ± 0.8	1.7 ± 0.5
-10 V; +15 V	2.3 ± 0.7	2.3 ± 0.5	2.7 ± 1.2	1.8 ± 0.7
-10 V; +20 V	1.0 ± 0.3	1.6 ± 0.7	2.3 ± 0.9	18 ± 6

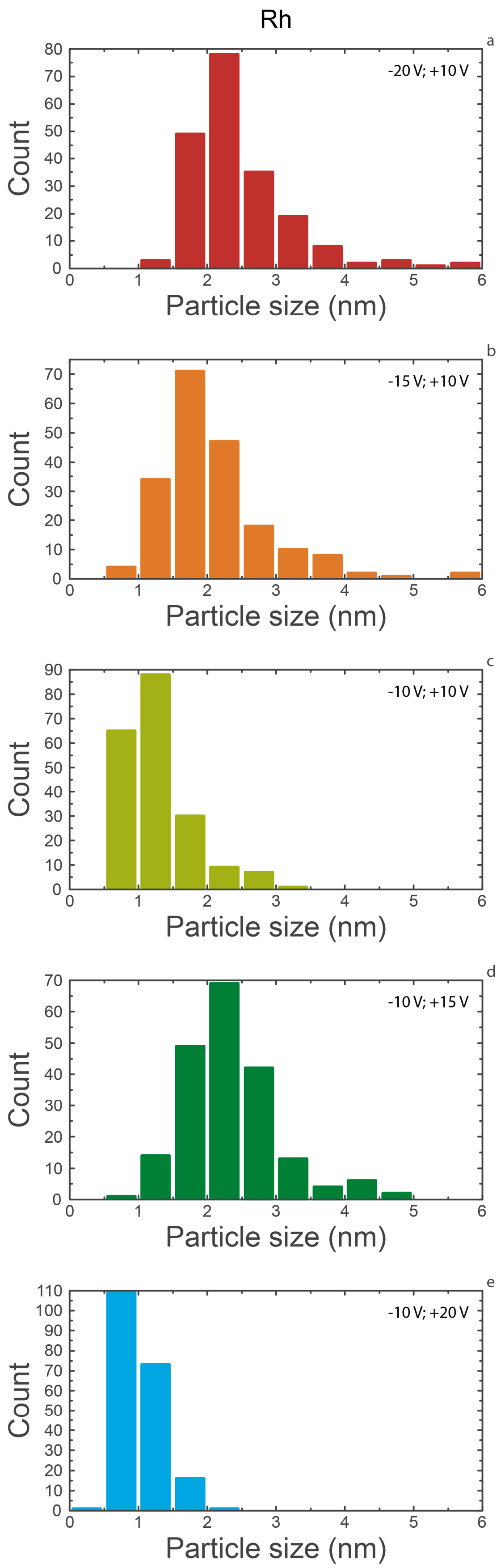

Fig. S3: Particle size distributions for studied Rh nanoparticles.

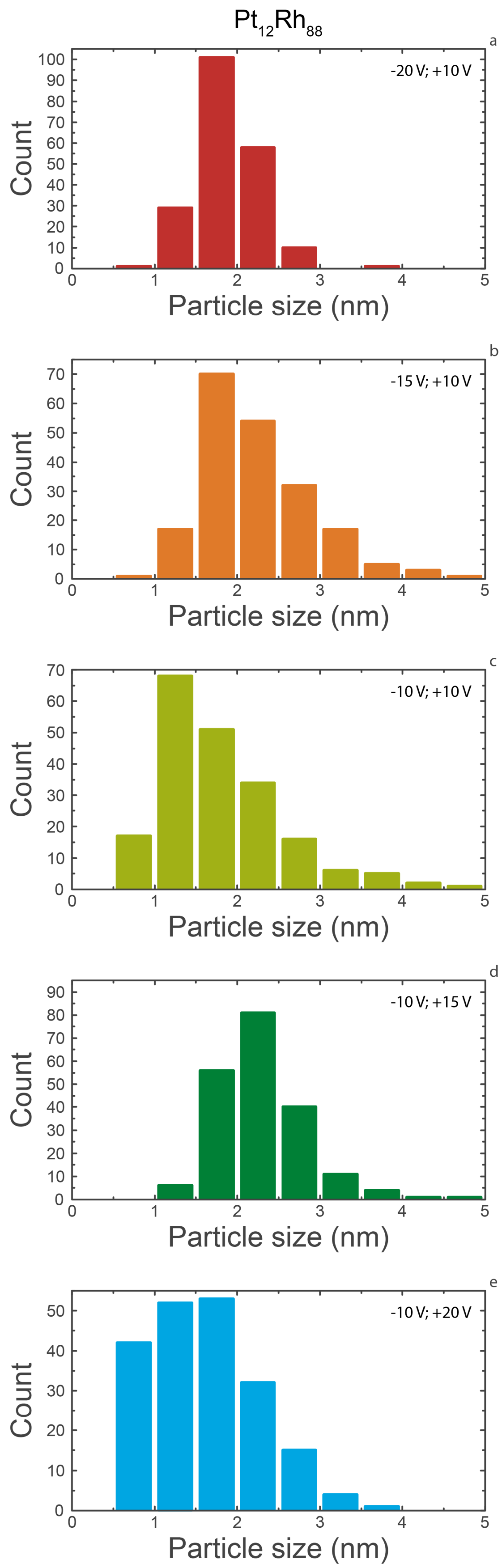

Fig. S4: Particle size distributions for studied $Pt_{12}Rh_{88}$ nanoparticles.

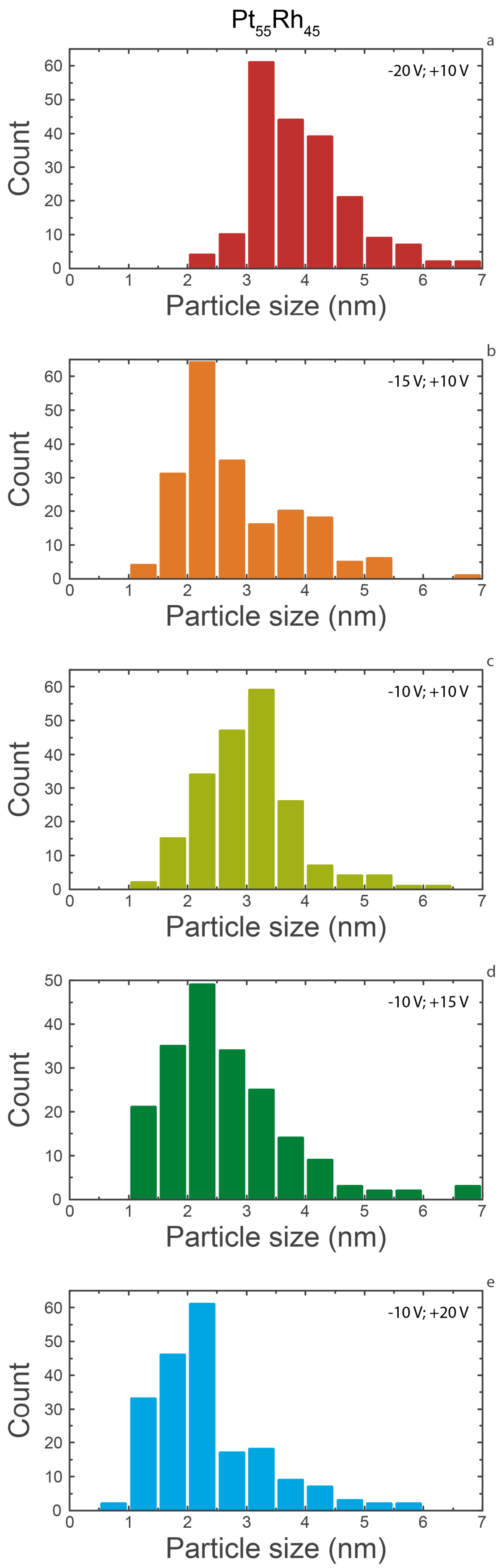

Fig. S5: Particle size distributions for studied $Pt_{55}Rh_{45}$ nanoparticles.

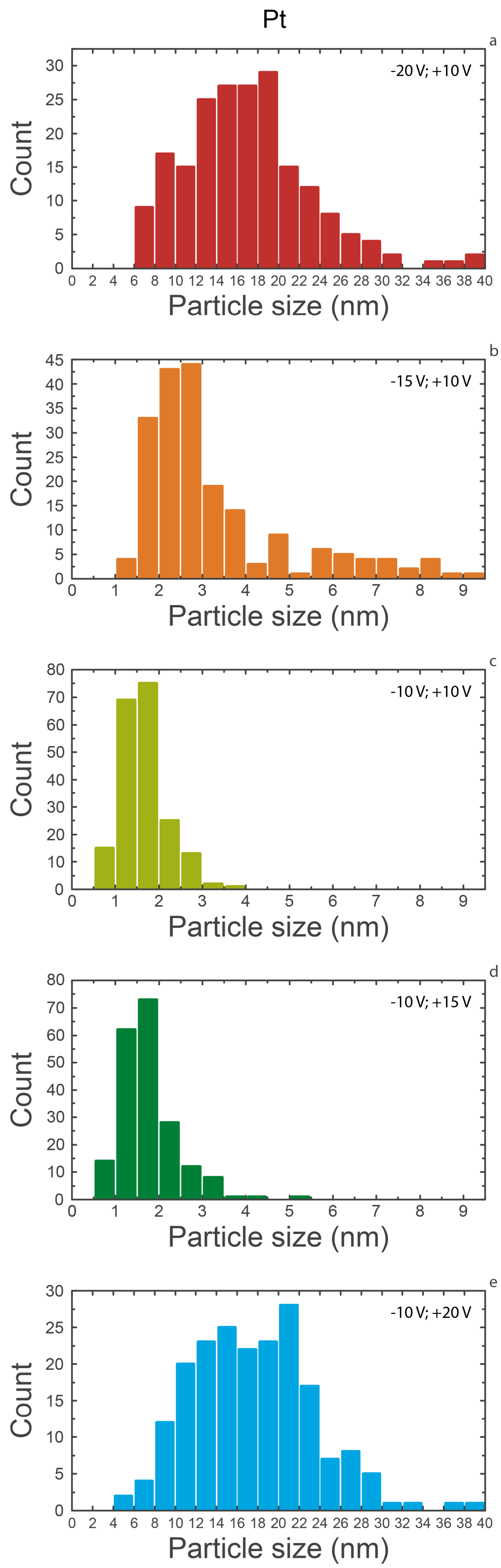

Fig. S6: Particle size distributions for studied Pt nanoparticles.

2D nanoparticle visualizations

This section provides 2D visualizations of the data presented in Fig. 4 of the main text. These visualizations, shown in Fig. S7, consist of one layer of rhodium and platinum atoms. As such, they are an approximation of a 2D cut through a nanoparticle.

For each model, containing 100 atoms, one can approximate the local Pt content that would be observed for these models through Rh k edge and Pt L_{III} edge EXAFS experiments. This is done by counting the number of neighboring platinum atoms ($n_{Pt,i}$) for each atom *i* in the model and dividing by the total number of neighboring atoms ($n_{t,i}$) for that atom *i*. For each atom, this yields the local relative platinum content ($x_{Pt,i}$):

$$x_{Pt,i} = \frac{n_{Pt,i}}{n_{t,i}} \cdot 100\% \qquad \text{(eq. 1)}$$

Averaging this value over either all platinum or all rhodium atoms will lead to an approximation of the Pt edge- and Rh edge-based platinum content, respectively.

The $Pt_{12}Rh_{88}$ surface in Fig. S7 gives a Pt edge-based platinum content of 25.0% and a Rh edge-based platinum content of 10.2%. In the $Pt_{55}Rh_{45}$ example, the Pt edge-based platinum content is 61.3% and the Rh edge-based platinum content is 51.2%. Though these numbers agree relatively well with the actual data, care should be taken when extrapolating these models as accurate reflections of 3-dimensional nanoparticles. Nonetheless, the two examples can be taken as reasonable first-order approximations of the average elemental distribution of the studied nanoparticles.

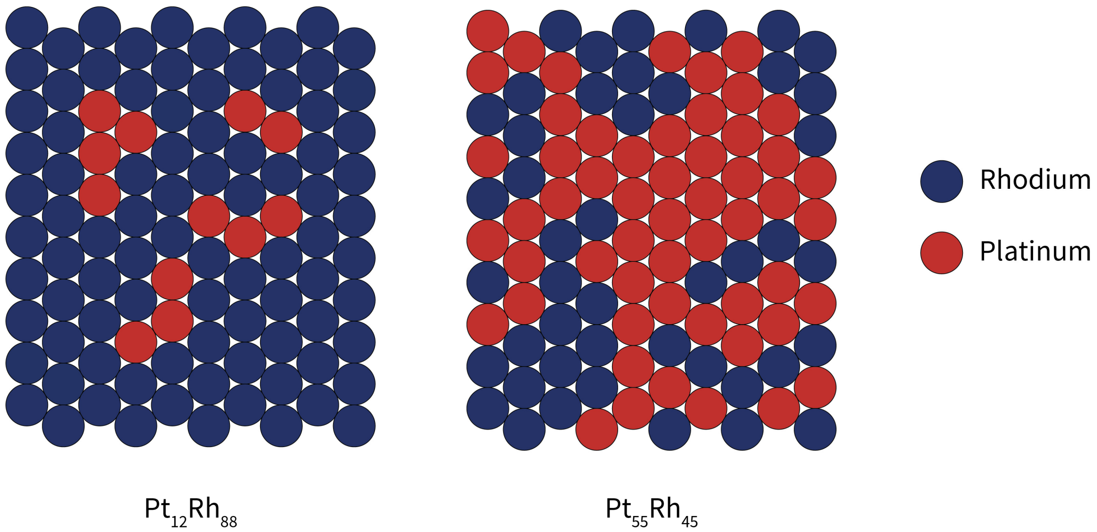

Fig. S7: 2D visualizations of the studied $Pt_{12}Rh_{88}$ and $Pt_{55}Rh_{45}$ nanoparticles.